Article

Experimental and Modelling Study of Controlled Release from Dextran-Based Cryogels

Carolina Lauriola [1], Laura Di Muzio [2], Patrizia Paolicelli [2], Maria Antonietta Casadei [2], Claudia Sergi [1], Jacopo Tirillò [1], Vito Cosimo Carriero [2] and Alessandra Adrover [1,*]

[1] Dipartimento di Ingegneria Chimica, Materiali e Ambiente, Sapienza Univerisità di Roma, 00184 Rome, Italy; carolina.lauriola@uniroma1.it (C.L.); claudia.sergi@uniroma1.it (C.S.); jacopo.tirillo@uniroma1.it (J.T.)

[2] Dipartimento di Chimica e Tecnologia del Farmaco, Sapienza Università di Roma, 00185 Rome, Italy; laura.dimuzio@uniroma1.it (L.D.M.); patrizia.paolicelli@uniroma1.it (P.P.); mariaanonietta.casadei@uniroma1.it (M.A.C.); vitocosimo.carriero@uniroma1.it (V.C.C.)

[*] Correspondence: alessandra.adrover@uniroma1.it

Abstract: In this work, five different dextran-based cryogels for controlled drug release are investigated. Vitamin B12 was used as a model drug for in vitro release tests. Two different drug-loading procedures were adopted, leading to very different drug release curves. Indeed, a fast Fickian release was observed when freeze-dried samples of $DEX_{40}PEG_{360}MA$ and $DEX_{40}PEG_{500}MA$ were infused with the drug after cryogel formation. On the contrary, a slowed highly non-Fickian behavior arises when the drug is loaded before the low-temperature crosslinking step, leading to the cryogel formation. The non-Fickian drug release, observed for all the five different dextran-based cryogels investigated, is actually due to the cryoconcentration phenomenon, modeled with a two-step release process. The proposed transport model accurately predicts experimental release curves characterized by a long lag time, confirming that dextran-based cryogels are suitable for controlled release.

Keywords: dextran-based cryogels; non-Fickian release; controlled release; cryoconcentration; transport modelling

1. Introduction

The use of polymeric systems for drug delivery purposes is becoming increasingly widespread [1–3]. Researchers focus on innovative systems that respond to the demand for cost-effectiveness, stability, simplicity and high efficacy [4–6]. In this regard, cryogels play a critical role [7–11]. In recent years, this old technology, which dates back to five decades ago, has been rediscovered due to its precious and unique properties. Cryogels share some features, such as a porous structure and superabsorbancy, with hydrogels [12–15]. Regardless, from multiple perspectives, cryogels represent an improved version of hydrogels. Specifically, they are characterized by an open interconnected macroporous structure, and consequently a higher surface area, and display optimal liquid absorption capacities and greater mechanical performance. On the contrary, hydrogels show a smaller pore size and low elasticity, which are not suitable for several applications [16,17]. The morphological and mechanical differences between hydrogels and cryogels arise from a distinct procedure of formation of the aforementioned scaffolds. As far as it concerns hydrogels, the polymerization and crosslinking process occur at room temperature. Cryogels, instead, are formed at a temperature below the freezing point of the solvent, and therefore polymerization and crosslinking occur in the interstitial spaces between the ice crystals, which are subsequently removed by freeze-drying or thawing processes. In this way, the space previously occupied by the ice crystals, which play the role of porogens, is replaced by the corresponding interconnected porous network. Although low temperatures reduce the kinetics of the polymerization and crosslinking reactions according to Arrhenius' law, the partial freezing of the solvent determines the concentration of the polymer solution—referred to as cryoconcentration—in

liquid microvolumes to the advantage of the gelation process. The choice of polymer, which can be natural or synthetic, is directly related to its field of application and influences the final texture, biodegradability and biocompatibility of the designed cryostructures. For instance, among natural polymers, the use of agarose, alginate [18–20], cellulose [21,22], chitosan [9,23–25], chondroitin [26,27], dextran [28–30] and gelatin [30–32] is a common practice. The potential to tune the physical and chemical properties of these macroporous sponge-like matrices has allowed them to be exploited for a wide variety of applications [33–39]. Cryogels are becoming very interesting in the pharmaceutical industry, where they can serve as carriers for the sustained release of drugs and even cells. Indeed, as reviewed in depth by Memic et al. [40], cryogels have been particularly investigated as injectable depots for local drug delivery, where release kinetics may be controlled by modifying the cryogel structure or incorporating other drug delivery modifiers into the scaffold. Therefore, a deeper understanding of the mechanism of drug release [41] from these delivery vehicles could help to optimize drug delivery systems and improve the safety and efficacy of therapies. Despite numerous studies attempting to model the release from polymeric matrices, including hydrogels [42–46], few articles have developed models that accurately describe the behavior of drug diffusion from cryogels [7,47–51]. The most applied models include the semi-empirical Higuchi and Korsmeyer–Peppas equations [52–55], which do not properly fit some experimental findings [30]. Moreover, previous studies have reported important differences in the release profiles from dextran-based cryogels and hydrogels, which were attributed to a cryoconcentration phenomenon affecting the drug during the cryogelation process [29]. Despite this effect, cryogels are not highly efficient for the sustained release of small molecules [56,57]. For this reason, different strategies have been proposed to better control the release behaviour of drugs from cryogels, including dextran-based cryogels [58]. Specifically, dextran has been combined with poly(N-isopropyl acrylamide) to develop thermoresponsive cryogels [59], with cyclodextrins [60] or with mesoporous bioactive glass [61]. Although these strategies proved to extend the drug release rate from dextran-based cryogels, better results will be achieved once the behavior of drug diffusion from cryogels can be accurately described.

In this paper, we propose a mechanistic model explaining the anomalous non-Fickian trend of release curves of vitamin B12 (cobalamin) from dextran-based cryogels. The non-Fickian behavior observed cannot be attributed to a Case II diffusion process [54,55], because the swelling process in cryogels is extremely fast and the release process occurs from a fully swollen sample. Depending on the drug-loading procedures adopted, we observed two different release behaviors: a fast Fickian release when freeze-dried samples were infused with the drug after cryogel formation, or a slowed highly non-Fickian behavior when the drug was loaded before the cryogelation process. The non-Fickian release, due to the cryoconcentration phenomenon, was modeled with a two-step release process that accurately predicts experimental release curves characterized by a long lag time and a slower release, suggesting the opportunity to exploit this attribute with a view to the controlled release of the drug. This aspect represents a determining factor for numerous therapies and several models have been proposed in the literature [62–64], but none of them refer explicitly to cryogels.

2. Materials and Methods

2.1. Materials

All used reagents were of analytical grade. Dextran (DEX) from *Leuconostoc mesenteroides* (Mn 40,000, DEX$_{40}$; Mn 500,000, DEX$_{500}$), hydroquinone mono-methyl ether, N,N′-carbonyldiimidazole (CDI), N-methyl-2-pyrrolidone, 4-dimethylaminopyridine (4-DMAP), anhydrous dimethylsulfoxide (DMSO), anhydrous tetrahydrofuran (THF), nicotinamide (NIC), ammonium persulfate (APS), N,N, N′, N′-tetramethylethylenediamine (TEMED), glycidyl methacrylate (GMA), hydroxyethyl methacrylate (HEMA), polyethylene glycol mono-methacrylate (Mn 360 and 500; PEG$_{360}$MMA and PEG$_{500}$MMA), deuterated water D$_2$O, dialysis membranes (cut-off 12–14 kDa), methanol for HPLC (MeOH), 2-

methoxyethanol and vitamin B12 were purchased from Sigma-Aldrich, St. Louis, MO, USA (Merck KGaA). Double-distilled water, absolute ethanol (EtOH), 2-methoxyethanol, acetic acid (CH_3COOH), 37% *w/w* hydrochloric acid (HCl), monobasic potassium phosphate (KH_2PO_4) and sodium hydroxide in pellets (NaOH) were purchased from Carlo Erba.

2.2. Synthesis of Dextran Methacrylate

The synthesis of $DEX_{40}MA$ was carried out as reported in previous studies [30,65]. DEX_{40} (2.5 g) was solubilized in anhydrous DMSO (20 mL) at room temperature under magnetic stirring for 24 h. After complete dissolution, 4-DMAP (0.71 g) and GMA (0.26 mL) were added. The reaction mixture was maintained under magnetic stirring at room temperature for 24 h. At the end of the reaction time, the solution was precipitated dropwise into 100 mL of absolute ethanol under continuous stirring. The precipitate underwent vacuum filtration and was redissolved in distilled water (30 mL). The solution was neutralized with HCl (1N). Subsequently, it was dialyzed against distilled water for three days and finally it was freeze-dried. To characterize the lyophilised polymer, ^{1}H-NMR analysis was performed with a Bruker Avance 400 spectrometer (Rheinstetten, Germany). The ^{1}H-NMR spectrum was recorded in D_2O and using NIC as the internal standard. For this purpose, 10 mg of polymer was dissolved in 0.4 mL of D_2O and 0.2 mL of NIC solution in D_2O (1 mg/mL). The obtained degree of methacrylation was $5 \pm 1\%$.

2.3. Synthesis of Dextran Derivatives

The other methacrylic derivatives of dextran were synthesized as described in previous works [66,67], with slight modifications. The synthesis procedure involved two steps. In the first one, 2-HEMA (0.29 g, 2.2 mmol), $PEG_{360}MMA$ (0.80 g, 2.2 mmol) or $PEG_{500}MMA$ (1.10 g, 2.2 mmol) was dissolved in anhydrous THF (7 mL) and, following this, CDI (0.37 g, 2.2 mmol) was added. The reaction was carried out under a nitrogen atmosphere for 16 h at room temperature. So, hydroquinone mono-methyl ether (0.12 g) was added to the intermediate and HEMA-IC (hydroxyethyl methacrylate N-imidazoylcarbamate) or PEGMA-IC (polyethylene glycol N-imidazoylcarbamate) was obtained after evaporating THF under reduced pressure conditions. In the second step, DEX (2.4 g, 14.8 mmol of glucose repetitive unit) was dissolved in anhydrous DMSO (18 mL in the case of DEX_{40} and 25 mL in the case of DEX_{500}) and the catalyst 4-DMAP (0.47 g, 3.85 mmol) was introduced. HEMA-IC or PEGMA-IC were added to the mixture without purification and the system was left to react for 24 h under magnetic stirring at room temperature. The reaction scheme of the synthesis of $DEX_{40}MA$ and dextran derivatives is reported in Supplementary Information, Figure S1A,B. The obtained mixture was precipitated dropwise in absolute ethanol (100 mL) for DEX_{40} and in methoxyethanol (150 mL) for DEX_{500}. The subsequent filtration allowed the separation of the solid phase which was dissolved in distilled water (20 mL for DEX_{40} and 40 mL for DEX_{500}) and neutralized with HCl (2 M) to avoid basic hydrolysis. The polymeric solution was dialyzed in distilled water, frozen and then lyophilized by using a LIO 5P freeze-dryer (5 Pascal, Milan, Italy). After the freeze-drying process, the polymers were characterized through ^{1}H-NMR analysis. The ^{1}H-NMR spectra were recorded in the presence of NIC used as the internal standard. ^{1}H-NMR samples were prepared by solubilizing 10 mg of polymer in 0.4 mL of D_2O and 0.2 mL of NIC solution in D_2O (1 mg/mL). The degree of derivatization DD% was calculated based on the peaks of the standard and of the methacrylic groups. The value of the achieved DD% was of $5 \pm 1\%$ for all the synthesized polymers. For an in-depth discussion of ^{1}H-NMR spectra of dextran derivatives, see [66].

2.4. Cryogel Preparation

Cryogels were prepared by a free radical crosslinking reaction in distilled water using the redox initiation system APS/TEMED. A certain amount of $DEX_{40}MA$, $DEX_{40}HEMA$, $DEX_{40}PEG_{360}MA$, $DEX_{40}PEG_{500}MA$ or $DEX_{500}PEG_{360}MA$, corresponding to 0.035 mmol of methacrylic groups, was dissolved in distilled water through magnetic stirring. Following

the complete solubilization of the polymer, APS (96 μL) and TEMED (54 μL) were added and after 30 s the systems were put into a cryostat (already set at the temperature of −12 °C) for two hours before undergoing the freeze-drying step. A pictorial representation of all the steps required for cryogel preparation is reported in Supplementary Information, Figure S2. The freeze-drying process was carried out with a LIO 5P bench freeze-dryer (5 Pascal, Italy) equipped with a vacuum pump Adixen (Alcatel, France). The polymer solutions were prepared in cylindrical glass molds (diameter 20 mm, height 40 mm) at room temperature. The final volume of the polymer solutions was 2 mL, which allowed us to obtain cylindrical lyophilized cryogel samples of 18.5 ± 0.5 mm diameter and 7.1 ± 0.2 mm height.

The method adopted for the preparation of cryogels is the result of an experimental campaign in which polymer concentration (6% *w/v*) and freezing temperature (−12 °C) were kept constant, whereas APS and TEMED concentrations were modified in order to vary the crosslinking rate of the polymer. We found out that we could obtain cryogel networks using APS concentrations in the range 1.5–13 mg/mL, and varying TEMED concentration according to APS, in order to keep the mmoles APS/mmoles TEMED ratio equal to 0.9 in all the cases. Based on these data, the cryogel systems investigated in this work were prepared by selecting an APS concentration within this range, specifically 2.4 mg/mL, which correspond to a mmoles APS/mmoles methacrylic groups ratio of 0.6. We are aware of the potential toxicity of the APS/TEMED redox initiation system and the need of cytotoxicity studies on the proprosed cryogel systems. However, it should be considered that one of the advantages of cryogels over the corresponding hydrogels is the need for smaller amounts of crosslinking reagents for network formation due to the cryoconcentration process. In light of this consideration, cryogels might be safer than the corresponding hydrogel systems. In any case, other biocompatible crosslinking methods can be applied to develop cryogel networks, such as those recently reviewed by Maiti et al. and Alavarse et al. [68,69], or safer alternatives to TEMED, such as those proposed by Pumford et al. [70]. We have not yet performed cytocompatiblity studies on these cryogels, although they are obviously possible, as sterile cryogels can be obtained by fabrication under aseptic conditions, with a standard procedure that requires that all the components of the pregel solution are sterilized separately, and then aseptically blended. This procedure, aimed at obtaining sterile cryogels, is usually adopted in all cases where final sterilization may cause substantial modification or degradation of the drug. We verified that the crosslinking reaction was completed after two hours. Indeed, we observed no differences between samples obtained by prolonging the cryogelation by up to four and six hours [30].

2.5. Absorption, Swelling and Degradation Studies

Absorption studies were performed with the intention of evaluating the maximum liquid uptake of the samples and the time required for complete swelling. For this purpose, phosphate buffer (PBS, pH 7.4) was preheated to the temperature of 37 °C and added dropwise to the surface of freeze-dried cryogels until a drop of PBS was observable at the bottom of the samples. The kinetics of swelling was determined by placing the samples in PBS (pH 7.4), kept in a thermostated water bath at the temperature of 37.0 ± 0.5 °C. The lyophilized specimens were left swelling until the swelling equilibrium was achieved. The water intake was tracked for 1 h. Specifically, at regular time intervals, cryogels were removed from the swelling medium and the excess of liquid was whipped off by percolation at atmospheric pressure. In this way, it was possible to weigh the samples. The swelling degree was evaluated as

$$Q(t) = \frac{M_{sw}(t)}{M_{dry}} \tag{1}$$

where $M_{sw}(t)$ is the weight (g) of the swollen sample at the time t and M_{dry} is the weight (g) of the dry sample. After the swelling studies, cryogels were left in PBS (pH 7.4) at 37.0 ± 0.5 °C and degradation rates were estimated. The samples were removed from the

medium at variable intervals of time to measure their weights and to evaluate their weight variation. This procedure was repeated until the complete sample degradation. All tests were conducted in triplicate.

2.6. Morphological Characterization

The internal architecture of freeze-dried cryogels was observed via a field-emission scanning electron microscope (FE-SEM) MIRA 3 by Tescan. Since the samples were characterized by low electrical conductivity, they were coated with a thin layer of gold to prevent electronic charging and to improve image quality. The coating process was carried out in vacuum conditions (0.4 mbar) for 2 min by a sputter coater Edwards S150B applying a voltage of 1 kV and an electrical current of 40 mA to the gold electrode.

2.7. Release of Vitamin B12

Release studies of vitamin B12 were conducted on $DEX_{40}PEG_{360}MA$, $DEX_{40}PEG_{500}MA$, $DEX_{40}MA$, $DEX_{40}HEMA$ and $DEX_{500}PEG_{360}MA$. A total of 2.5 mg of the drug was loaded on cryogel samples prepared with 120 mg of polymer, giving an approx. 50 (w/w) polymer/drug ratio, to ensure limited drug interference with the crosslinking process.

Two different loading procedures were implemented:

1. Loading before cryogel formation (pre-loading)
    Cryogels were loaded with 2.5 mg of vitamin B12 by introducing a solution of vitamin B12 in distilled water (2.5 mg/mL) directly into the system before the low-temperature crosslinking step, which was carried out as reported in Section 2.4, leading to the cryogel formation.
2. Loading on preformed cryogel (after loading)
    Freeze-dried cryogel samples were infused with a solution of vitamin B12. The concentration of the solution was arranged so that, on the base of absorption volumes, the amount of vitamin B12 in the cryogel was 2.5 mg. After loading, the specimens were lyophilized.

Each scaffold was placed in 20 mL of PBS (pH 7.4) under mild magnetic stirring. Temperature was maintained at 37.0 ± 0.5 °C by a water bath. At defined intervals of time, aliquots of 250 µL of the release medium were taken and immediately replaced with an identical volume of fresh PBS, so that the reservoir volume (20 mL) remained constant. Withdrawals were made every minute for the first 5 min, then every 5 min up to 20 min, every 10 min until the first hour passed, every 30 min up to 2 h and then every hour up to 8 h. The last two aliquots were withdrawn after 24 and 48 h. The concentration c_{res} of the released drug in the reservoir volume was evaluated by HPLC analysis. The HPLC consisted of a Perkin Elmer Series 200 LC pump, supplemented with a 235 Diode Array Detector and equipped with a Merck Hibar LiChrocart (250-4, 5 µm) RP-18 column. A 65:35 mixture of 0.01 M CH_3COOH/MeOH was used as the eluent. The flow rate was set to 0.7 mL/min. Aliquots of 25 µL of every sample solution were injected into the HPLC system. A calibration curve c[mg/mL] = 0.0465A[V × s], valid in the concentration range $c \in [0.0005, 0.16]$ mg/mL and reported in Supplementary Information Figure S3, was constructed to quantify the concentration of vitamin B12 in the reservoir at each withdrawal time instant ($\lambda_{max} = 361$ nm). All experiments were conducted in triplicate. Release profiles were reported as c_{res} vs. t and M_t/M_∞ vs. time t [min] (amount of drug released up to time t rescaled onto the total amount of drug released after an infinite time) with the corresponding standard deviations.

3. Results and Discussion

3.1. Swelling and SEM Analysis

Figure 1a shows the swelling degree $Q(t)$ of the $DEX_{40}PEG_{360}MA$ and $DEX_{40}PEG_{500}MA$ cryogels as a function of time t. Almost complete swelling is attained within 2 min for both cryogels, which also share a comparable degradation time, as shown in Figure 1b. The swelling data are reported in Figure 1a for the first 20 min in order to better show the rapid

saturation on the asymptotic values which remain essentially unchanged until the end of the experiment (1 h). Figure 2 shows a picture of a DEX$_{40}$PEG$_{360}$MA cryogel before (a) and after complete swelling (b).The degradation data shown in Figure 1b have larger errors than swelling data (as highlighted by the error bars) intrinsically due to the experimental procedure, but show a well-defined decaying behavior, with a total degradation time of 35 days for both cryogels.
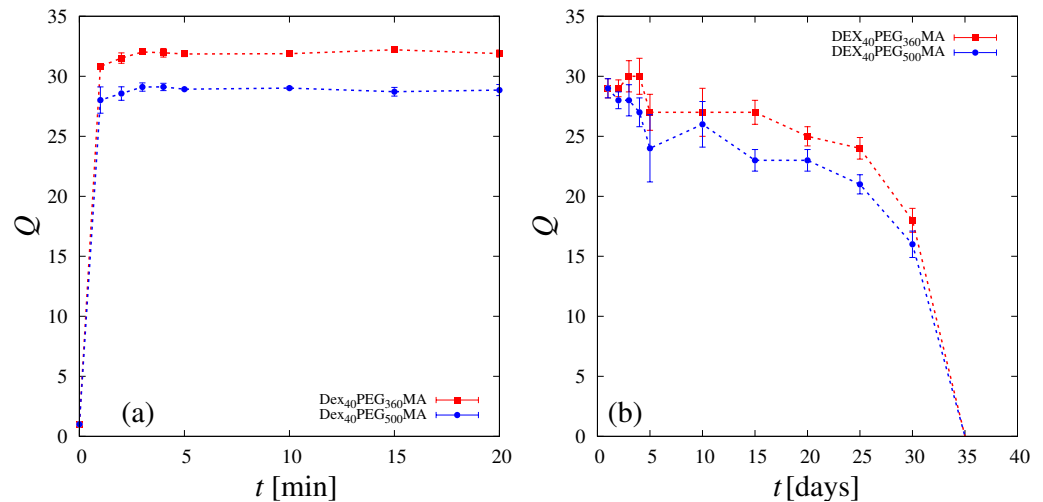

Figure 1. Swelling degree curves (**a**) and degradation curves (**b**) of freeze-dried DEX$_{40}$PEG$_{360}$MA cryogels and DEX$_{40}$PEG$_{500}$MA cryogels.
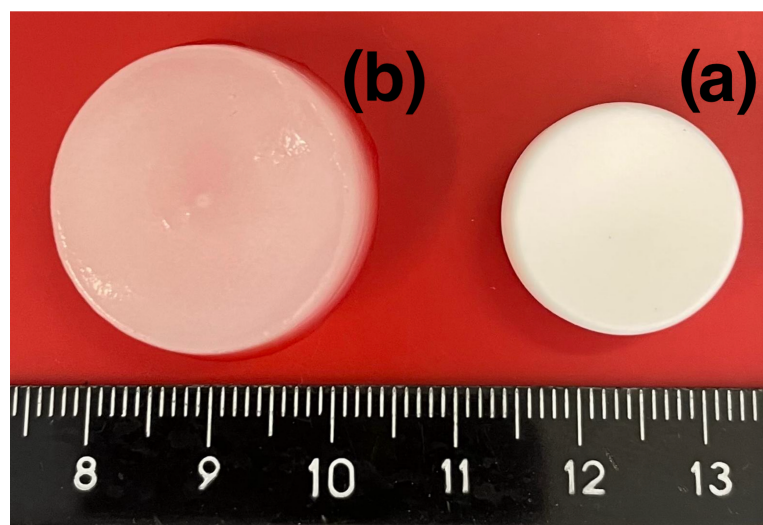
Figure 2. Freeze-dried DEX$_{40}$PEG$_{360}$MA cryogel before (**a**) and after complete swelling (**b**).

It can be observed that a slightly lower equilibrium swelling degree is observable for DEX$_{40}$PEG$_{500}$MA. It can be attributed to the formation of clusters between the oxyethylene units, resulting in a greater degree of interaction between the polymer chains and the formation of conglomerates which, in turn, determine the smaller mesh of the polymer network and a lower capability of solvent penetration, as shown by SEM analysis in Figure 3a,b. Indeed, during freeze concentration, the dextran/PEG concentrations might become high enough for phase separation to occur, thus forming dextran and PEG clusters, as observed by Heller et al. [71].
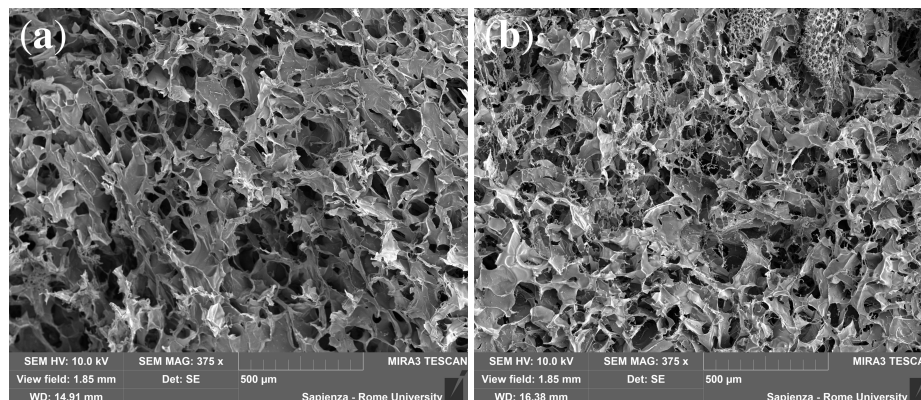
Figure 3. SEM images showing the morphology of cryogels. (**a**) $DEX_{40}PEG_{360}MA$. (**b**) $DEX_{40}PEG_{500}MA$.

3.2. Release Studies

Release curves, shown in Figure 4a for $DEX_{40}PEG_{360}MA$ and in Figure 4b for $DEX_{40}PEG_{500}MA$, are highly sensitive to the drug-loading procedure. Specifically, for both cryogels analyzed, the release curve for the after-loaded drug is significantly faster than that obtained with the pre-loaded drug. Moreover, the after-loaded release curve exhibits, for both cryogels, a well-defined power-law behavior $M_t/M_\infty \sim t^n$ at a short–intermediate time-scale, characterized by an exponent $n = 0.55$ close to $n = 0.5$ characterizing the Fickian behavior [54]. On the contrary, the pre-loaded release curves exhibit a markedly non-Fickian behavior characterized by an exponent n significantly larger than 0.5; specifically, $n = 0.8$ for $DEX_{40}PEG_{360}MA$ and $n = 1.2$ for $DEX_{40}PEG_{500}MA$. The larger the value of the n exponent, the longer the lag time observed in the release curves [64].
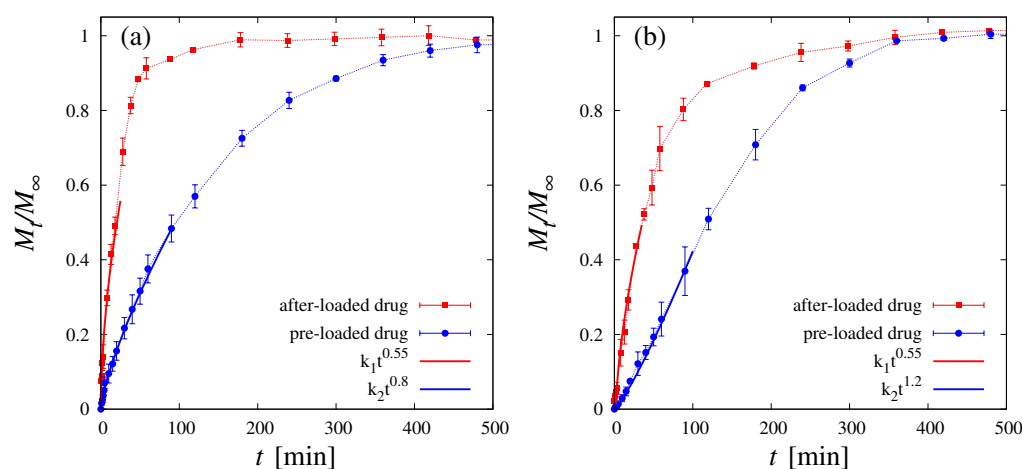
Figure 4. Release curves of vitamin B12 in the case of pre-loaded drug (blue curves) and after-loaded drug (red curves). (**a**) Release from $DEX_{40}PEG_{360}MA$ cryogel. (**b**) Release from $DEX_{40}PEG_{500}MA$ cryogel.

A similar non-Fickian behavior was already observed for methacryloyl gelatin (GelMA) blended with dextran methacrylate ($DEX_{40}MA$) cryogels [30] and explained as a consequence of the cryoconcentration phenomenon. Indeed, the cryogel can be viewed as a hierarchical porous structure characterized by the coexistence of two phases, a microporous dense stationary one, in which the drug (in the pre-loaded case) gets trapped during the cryogelation process, and a macroporous "mobile" one. During the release process, the cryogel sample rapidly swells, and the drug, initially trapped in the microporous phase, is irreversibly released in the macroporous phase where it is free to diffuse out of the sample. Therefore, the release process in the pre-loading case occurs in two steps characterized by two different time-scales: the time-scale t_t, associated with the internal drug-transfer process from the stationary to the mobile phase (controlling the lag time), and the time-scale t_d,

associated with diffusive transport in the macroporous phase. The interplay between these two transport processes is responsible for the observed non-Fickian behavior of the release curves if the drug is pre-loaded. On the contrary, if the drug is infused in the lyophilized sample after the cryogel formation (after-loading procedure), there is no drug trapping in the microporous phase (absence of the cryoconcentration phenomenon) and drug release occurs exclusively by diffusive transport in the macroporous phase. By considering that the swelling process is extremely fast, compared to the diffusional time-scale, the release curves exhibit a typical Fickian behavior, as experimentally observed.

In the presence of cryoconcentration, the more pronounced non-Fickian behavior of $DEX_{40}PEG_{500}MA$ with respect to $DEX_{40}PEG_{360}MA$ is due to a larger fraction of the drug initially being trapped in the microporous phase. This finding is in agreement with the reduced swelling capability of $DEX_{40}PEG_{500}MA$ due to the formation of clusters between the oxyethylene units, resulting in a greater degree of interaction between the polymer chains and the formation of conglomerates, as shown by SEM images.

3.3. Theoretical Model of Drug Release in the Pre-Loading Case

The transport model developed is based on the coexistence of two phases: a microporous stationary phase, in which the vitamin is initially concentrated due to the cryoconcentration phenomenon, and a macroporous mobile phase where drug transport occurs exclusively by diffusion. Indeed, the swelling process of the lyophilized sample is extremely fast (in the order of 2 min to reach equilibrium conditions) so that the cryogel is assumed to be fully swollen at the beginning of the release process. For this reason, the non-Fickian release observed cannot be attributed to a Case II transport process [54,55], in which drug release and swelling are two phenomena occurring simultaneously. When $R_{sw} \simeq 13$ mm and $H_{sw} \simeq 10$ mm are the dimensions (radius and height) of the swollen cylindrical sample (volume $V_{cyl} = \pi R_{sw}^2 H_{sw}$) and $m_0 \simeq 2.5 \pm 0.1$ mg is the amount of drug loaded in the cryogel, the initial drug concentration in the specimen is $c_0 = m_0/V_{cyl} \simeq 0.47$ mg/mL.

The drug trapped in the microporous phase, with the initial concentration $c_s(r,z,0) = \varepsilon_0 c_0$, is irreversibly released in the macroporous mobile phase with a linear transfer rate $k_t c_s$, directly proportional to the local drug concentration $c_s(r,z,t)$. The fraction ε_0 of drug initially trapped in the microporous phase is one important parameter of the model as well as the transfer coefficient $k_t [s^{-1}]$ controlling the time-scale $t_t = 1/k_t$ associated with the internal drug-transfer process between phases. Once in the mobile phase, the drug is free to diffuse out of the sample into the liquid reservoir (volume V_{res}) where perfect mixing conditions are ensured by agitation.

Let $c_m(r,z,t)$ and $c_{res}(t)$ be the drug concentrations in the mobile phase and in the reservoir, respectively, with the initial conditions $c_m(r,z,0) = (1-\varepsilon_0)c_0$ and $c_{res} = 0$. The coupled balance equations for c_s, c_m and c_{res} read as

$$\frac{\partial c_s(r,z,t)}{\partial t} = -k_t c_s \tag{2}$$

$$\frac{\partial c_m(r,z,t)}{\partial t} = D_{B12}\nabla^2 c_m + k_t c_s \tag{3}$$

$$c_m(r,z,t)\Big|_S = c_{res}(t), \quad \frac{\partial c_m}{\partial r}\Big|_{r=0} = 0 \tag{4}$$

$$V_{res}\frac{\mathrm{d}c_{res}(t)}{\mathrm{d}t} = D_{B12}\int_S -\nabla c_m \cdot \mathbf{n}\, ds - \sum_{i=1}^{N_w^t} V_w c_{res}\delta(t - t_w^i) \tag{5}$$

where $\delta(t)$ is a Dirac delta function, $\nabla(\cdot) = (\frac{\partial \cdot}{\partial r}, \frac{\partial \cdot}{\partial z})$ and $\nabla^2(\cdot) = \frac{\partial^2 \cdot}{\partial z^2} + \frac{1}{r}\frac{\partial}{\partial r}\left(r\frac{\partial \cdot}{\partial r}\right)$ are the gradient and Laplacian operators in cylindrical coordinates, S is the lateral surface of the cylindrical specimen, $\mathbf{n}$ is the outward unit normal vector of S and D_{B12} is the diffusion coefficient of B12 in PBS in the macroporous phase.

Numerical results for the concentration fields were obtained by solving the transport scheme with a commercial software enforcing the Finite-Element Method (Comsol 5.5).

For the numerical integration of the coupled time-dependent transport equations of c_s and c_m, the Coefficient Form PDE package was adopted for the 2-d axial symmetric geometry (cylinder) and solved in transient conditions (time-dependent solver, fully coupled method) together with the ODE for c_{res}. Lagrangian quadratic elements were chosen. The MUMPS solver was adopted with the relative tolerance 10^{-6}.

The time-dependent Dirichlet boundary condition, Equation (4), replaces the generally adopted perfect sink condition ($c_m|_S = 0$) that is not appropriate for describing our experiments in which the ratio α

$$\alpha = V_{cyl}/V_{res} \tag{6}$$

is about $1/4$ and therefore is not small enough for the perfect sink approximation to be valid ($\alpha \ll 1$). Increasing the volume of the reservoir is to be avoided, as the concentration of the drug, at the first withdrawals, would be too low and also would worsen the mixing conditions in the reservoir.

The adoption of Equation (4) for c_m at the boundary S requires the introduction of the balance Equation (5) for c_{res}. Equation (5) takes into account the finite volume of the reservoir and the N_w withdrawals (each with volume V_w) that are made at different time instants $\{t_w^i\}_{i=1}^{N_w}$ in order to measure, by HPLC, the drug concentration in the reservoir $c_{res}(t_i)$ at the withdrawal time t_i and build up the experimental $M_t(t_i)$ vs. t_i release curve

$$M_t(t_i) = c_{res}(t_i)V_{res} + \sum_{j=1}^{N_w^t} c_{res}(t_j)V_w \tag{7}$$

where N_w^t denotes the number of withdrawals made from time $t = 0$ to time t (or equivalently t_i). Equation (7) can be also adopted to evaluate the amount of drug $M_t(t)$ released up to time t from the transport model Equations (2)–(5), by simply replacing $c_{res}(t_i)$ with $c_{res}(t)$.

The finite value of α and the withdrawals influence the total amount of drug M_∞ that can be asymptotically released [72,73]. Indeed, according to Equation (7), M_∞ attains the form

$$M_\infty = c_{res}^\infty V_{res} + \sum_{j=1}^{N_w} c_{res}(t_j)V_w = \frac{c_0 V_{cyl}}{1+\alpha} + \frac{\alpha}{1+\alpha} \sum_{j=1}^{N_w} c_{res}(t_j)V_w \tag{8}$$

where $c_{res}^\infty = (c_0 V_{cyl} - \sum_{j=1}^{N_w^t} c_{res}(t_j)V_w)/(V_{cyl} + V_{res})$ is the asymptotic concentration in the reservoir, coinciding with the uniform drug concentration c_m^∞ that asymptotically sets in the mobile phase when all components of the concentration gradient nihilate ($\nabla c_m = \mathbf{0}$), and the drug release from the specimen to the reservoir stops. From Equation (8), it can be readily observed that, the larger is the value of α, the more M_∞ deviates from (and is smaller than) $m_0 = c_0 V_{cyl}$. On the contrary, the effect of the withdrawals is to increase the amount of drug asymptotically released.

Given the large porosity of the cryogels and the relatively small molecular weight of B12, the diffusion coefficient D_{B12} can be assumed to be close to the bare diffusion coefficient of B12 in PBS. Specifically, we assumed $D_{B12} = 7.2 \times 10^{-10}$ m^2/s for both the DEX$_{40}$PEG$_{360}$MA and DEX$_{40}$PEG$_{500}$MA cryogels. See Section 3.4 for a detailed analysis of the physical/mathematical considerations supporting this choice.

The two parameters to tune in order to fit the experimental data are the fraction ε_0 of B12 initially trapped in the microporous phase and the transfer rate coefficient k_t. The best-fit value for k_t is $k_t = 2.6 \times 10^{-4}$ s^{-1} for both cryogels. The two cryogels differ in the amount of vitamin initially trapped in the microphase, namely $\varepsilon_0 = 0.80$ for DEX$_{40}$PEG$_{360}$MA and $\varepsilon_0 = 0.95$ for DEX$_{40}$PEG$_{500}$MA. This difference, as in the case of the equilibrium swelling degree, could be explained by the larger amount of conglomerates in the DEX$_{40}$PEG$_{500}$MA due to a stronger interaction between the chains. This results in a smaller mesh size of the polymer network, which then traps a larger fraction of the drug.

The excellent agreement between model predictions and experimental release curves for $DEX_{40}PEG_{360}MA$ and $DEX_{40}PEG_{500}MA$ in the pre-loaded case is shown in Figure 5.
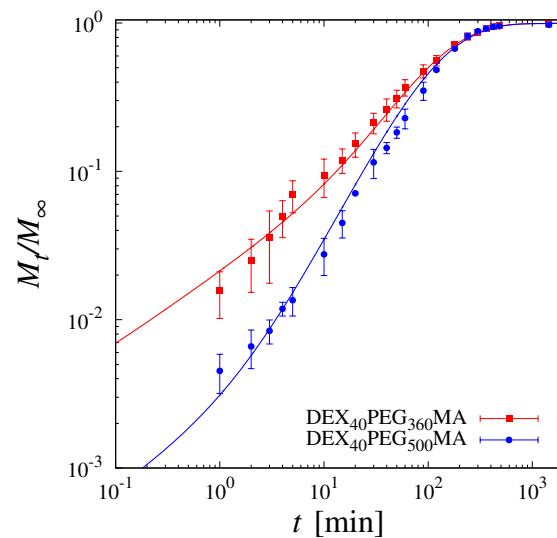
Figure 5. Log−log plot of release data of vitamin B12 (pre-loaded) from $DEX_{40}PEG_{360}MA$ and $DEX_{40}PEG_{500}MA$ cryogels. Continuous lines indicate model predictions.

Figure 5 clearly shows how the model is capable of describing the lag time and the non-Fickian behaviour of the release curves, as well as the long-term saturation towards the complete release. As a further confirmation, Figure 6 shows a quantitative comparison between the experimental values of c_{res} at different withdrawal time instants t_i and model predictions.
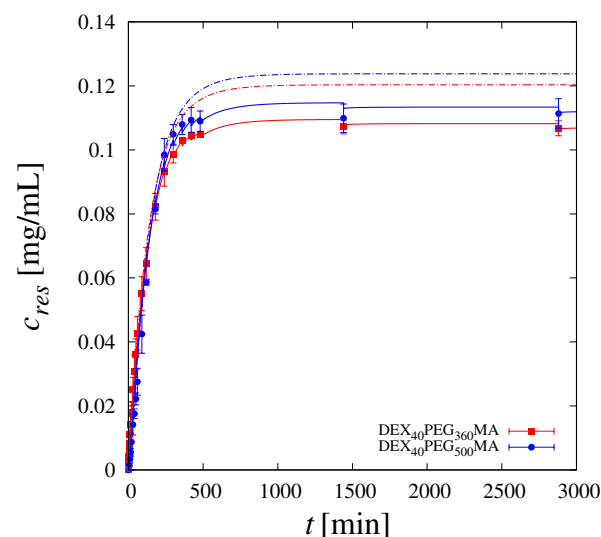
Figure 6. Comparison between experimental results for $c_{res}(t_i)$ (points) and model predictions. Continuous lines are numerical results accounting for the effect of withdrawals on release dynamics. Dashed lines are numerical results neglecting the effect of withdrawals on release dynamics.

Figure 6 allows us to appreciate the importance of taking into account the effect of withdrawals on release dynamics [72,73]. Indeed, each withdrawal (and subsequent replenishment of the same aliquot with fresh solution) results in an immediate decrease in the drug concentration in the reservoir, and this affects the release dynamics, especially in the case of frequent withdrawals on intermediate time-scales. Actually, Figure 6 shows the excellent agreement between the experimental data and model predictions when

withdrawals are properly accounted for (continuous lines). On the contrary, a significant deviation between the experimental data and model predictions (dashed lines) can be observed if withdrawals are neglected in the dynamics of c_{res}. Neglecting withdrawals in modeling the release dynamics is possible, but this may lead to significant errors in the estimate of transport parameters, namely k_t and ε_0.

Finally, it is worth noting that the best-fit values of the transfer rate coefficient k_t implies a value of the Damkölher number Da in the order of ten. Specifically,

$$Da = \frac{t_d}{t_t} = \frac{\frac{(H_{sw}/2)^2}{D_m}}{\frac{1}{k_t}} = \frac{k_t(H_{sw}/2)^2}{D_{B12}} \simeq 9 \tag{9}$$

By considering that Da represents the ratio between the characteristic diffusion time t_d and the characteristic transfer time t_t, a value of Da significantly larger than unity implies that the internal drug transfer between the micro- and the macrophase is a fast process, controlling the temporal evolution of the release curves at short/intermediate time-scales. On the contrary, the long-term behavior is controlled by drug diffusion in the macroporous phase, and this allows us to estimate the value of the diffusion coefficient D_{B12}, as discussed in detail in Section 3.4.

The interplay between internal transfer and diffusion in the mobile phase, at short intermediate time-scales, is responsible for the non-Fickian behaviour, more pronounced for DEX$_{40}$PEG$_{500}$MA because a larger fraction of drug is initially trapped in the stationary phase. The non-Fickian behavior of the release curve is a common feature of many dextran-based cryogels when the drug is loaded before the cryogelation process. Indeed, Figure 7 shows the release curves M_t/M_∞ vs. t of pre-loaded B12 for DEX$_{40}$MA, DEX$_{40}$HEMA and DEX$_{500}$PEG$_{360}$MA. The corresponding raw release data c_{res} vs. t are shown in Supplementary Information, Figure S4.
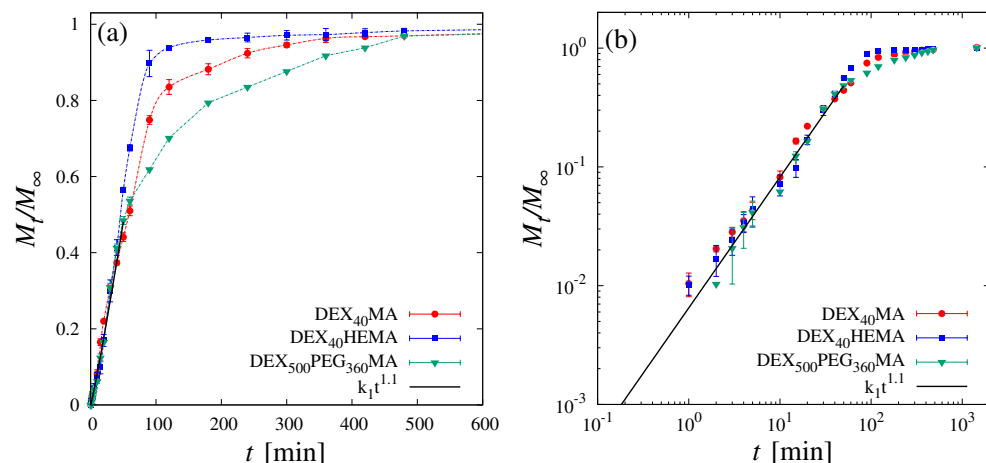
Figure 7. (**a**,**b**) M_t/M_∞ vs. t for pre-loaded B12 from DEX$_{40}$MA, DEX$_{40}$HEMA and DEX$_{500}$PEG$_{360}$MA cryogels. The continuous black line highlights the non-Fickian behavior $M_t/M_\infty \sim t^n$ with $n = 1.1$.

The log–log plot allows us to highlight the non-Fickian behavior characterized by an exponent $n = 1.1$ for all these dextran-based cryogels. The B12 release is characterized by the same lag time for all the cryogels, and represents the fingerprint of drug trapping in the stationary phase induced by the cryoconcentration process.

3.4. Estimation of the Diffusion Coefficient D_{B12}

On a long time-scale, when the release process is controlled solely by drug diffusion in the macroporous phase, the fraction of unreleased drug $1 - M_t/M_\infty$ in the cylindrical sample decays exponentially over time t as

$$1 - \frac{M_t}{M_\infty} \sim e^{-D_{B12}\, t \lambda_0^2}, \quad \lambda_0^2 = \alpha_1^2 + \frac{\pi^2}{H_{sw}^2} \tag{10}$$

where λ_0^2 is the first (dominant) eigenvalue of the Laplacian operator ∇^2 in cylindrical coordinates with homogeneous Dirichlet boundary conditions and α_1 is the first positive root of the J_0 Bessel function $J_0(\alpha_1 R_{sw}) = 0$. For the dimensions R_{sw} and H_{sw} of the swollen samples under investigation, the dominant eigenvalue λ_0 is equal to $\lambda_0 = 13.571 \times 10^4$ [m^{-2}].

Figure 8 shows the decay of $1 - M_t/M_\infty$ vs. t for both cryogels DEX$_{40}$PEG$_{360}$MA and DEX$_{40}$PEG$_{500}$MA and for both loading conditions (before and after cryogel formation). The log-normal scale adopted highlights that, on long time-scales, the trend is indeed an exponential decay over time, characterized by the same exponent for all the curves. By best-fitting the experimental exponential decay of $1 - M_t/M_\infty$ vs. t with Equation (10), it is possible to estimate the diffusion coefficient D_{B12} in the macroporous phase, thus obtaining $D_{B12} = (7.17 \pm 0.3) \times 10^{-10}$ m^2/s. The long-term exponential decay is the same for all the curves, whether the drug was loaded before cryogel formation or after cryogel formation by infusion. This confirms that the lag effect observed in the release curves in the case of pre-loaded drugs is due solely to the entrapment of the drug in the stationary phase by cryoconcentration.
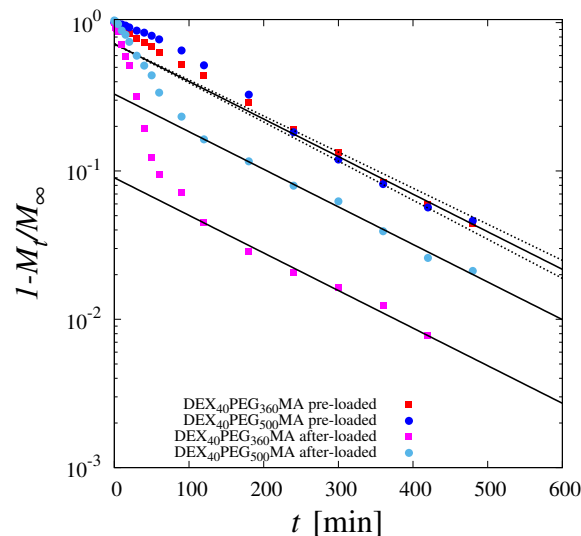
Figure 8. Log−normal plot of $1 - \frac{M_t}{M_\infty}$ vs. t for DEX$_{40}$PEG$_{360}$MA and DEX$_{40}$PEG$_{500}$MA for both drug loading conditions (before and after cryogel formation). Continuous lines indicate the exponential decay, Equation (10), with $D_{B12} = (7.17 \pm 0.3) \times 10^{-10}$ m^2/s. Dashed lines highlight the confidence interval.

4. Conclusions

This study demonstrates the potential of dextran-based cryogels for controlled drug release applications, using vitamin B12 as a model drug for in vitro release tests. The research highlights how different drug loading procedures significantly influence the release kinetics. Specifically, freeze-dried samples infused with the drug after cryogel formation exhibit a fast Fickian release. In contrast, when the drug is loaded before the low-temperature crosslinking step that leads to cryogel formation, a slowed, highly non-Fickian release behavior is observed. This non-Fickian release is attributed to the cryoconcentration phenomenon and is accurately modeled using a two-step release process. The mechanistic

model proposed in this study successfully explains the anomalous non-Fickian release trends, distinguishing it from other diffusion processes such as Case II diffusion. This study highlights the importance of the drug loading procedure in tailoring drug release profiles from cryogels, offering valuable insights for the development of controlled-release therapies. The cryogels proposed in this work may also be suitable for drug molecules of higher molecular weight. Indeed, we have already reported on the possibility of applying these dextran derivatives for the development of injectable and in situ gelling drug delivery systems, specifically designed for the controlled release of large molecules [66]. Certainly, the carbonate ester makes these polymer networks easily degradable in vivo. Therefore, these dextran derivatives can certainly also be proposed for the delivery of high-molecular-weight drugs with cryogel systems.

References

1. Calori, I.R.; Braga, G.; de Jesus, P.d.C.; Bi, H.; Tedesco, A.C. Polymer scaffolds as drug delivery systems. *Eur. Polym. J.* **2020**, *129*, 109621. [CrossRef]
2. de Castro, J.M.C.K.C.; Campos, M.G.N. Drug-loaded polymeric nanoparticles: A review. *Int. J. Polym. Mater. Polym. Biomater.* **2022**, *71*, 1–13. [CrossRef]
3. Abasian, P.; Ghanavati, S.; Rahebi, S.; Khorasani, S.N.; Khalili, S. Polymeric nanocarriers in targeted drug delivery systems: A review. *Polym. Adv. Technol.* **2020**, *31*, 2939–2954. [CrossRef]
4. Hamidi, M.; Azadi, A.; Rafiei, P. Hydrogel nanoparticles in drug delivery. *Adv. Drug Deliv. Rev.* **2008**, *60*, 1638–1649. [CrossRef]
5. Gholamali, I.; Yadollahi, M. Bio-nanocomposite polymer hydrogels containing nanoparticles for drug delivery: A review. *Regen. Eng. Transl. Med.* **2021**, *7*, 129–146. [CrossRef]
6. Laracuente, M.L.; Marina, H.Y.; McHugh, K.J. Zero-order drug delivery: State of the art and future prospects. *J. Control. Release* **2020**, *327*, 834–856. [CrossRef] [PubMed]
7. Öncel, P.; Çetin, K.; Topçu, A.A.; Yavuz, H.; Denizli, A. Molecularly imprinted cryogel membranes for mitomycin C delivery. *J. Biomater. Sci. Polym. Ed.* **2017**, *28*, 519–531. [CrossRef]
8. Newland, B.; Varricchio, C.; Körner, Y.; Hoppe, F.; Taplan, C.; Newland, H.; Eigel, D.; Tornillo, G.; Pette, D.; Brancale, A.; et al. Focal drug administration via heparin-containing cryogel microcarriers reduces cancer growth and metastasis. *Carbohydr. Polym.* **2020**, *245*, 116504. [CrossRef]
9. Evans, C.; Morimitsu, Y.; Hisadome, T.; Inomoto, F.; Yoshida, M.; Takei, T. Optimized hydrophobically modified chitosan cryogels for strength and drug delivery systems. *J. Biosci. Bioeng.* **2021**, *132*, 81–87. [CrossRef]
10. Ari, B.; Sahiner, M.; Suner, S.S.; Demirci, S.; Sahiner, N. Super-macroporous pulluan cryogels as controlled active delivery systems with controlled degradability. *Micromachines* **2023**, *14*, 1323. [CrossRef]
11. Hakami, A.; Narasimhan, K.; Comini, G.; Thiele, J.; Werner, C.; Dowd, E.; Newland, B. Cryogel microcarriers for sustained local delivery of growth factors to the brain. *J. Control. Release* **2024**, *369*, 404–419. [CrossRef] [PubMed]
12. Jahanmir, G.; Chau, Y. Chapter 9—Mathematical models of drug release from degradable hydrogels. In *Biomedical Applications of Nanoparticles*; Grumezescu, A.M., Ed.; William Andrew Publishing: Norwich, NY, USA, 2019; pp. 233–269. [CrossRef]
13. Sung, Y.K.; Kim, S.W. Recent advances in polymeric drug delivery systems. *Biomater. Res.* **2020**, *24*, 12. [CrossRef] [PubMed]

14. Bordbar-Khiabani, A.; Gasik, M. Smart Hydrogels for Advanced Drug Delivery Systems. *Int. J. Mol. Sci.* **2022**, *23*, 3665. [CrossRef] [PubMed]

15. Liu, B.; Chen, K. Advances in Hydrogel-Based Drug Delivery Systems. *Gels* **2024**, *10*, 262. [CrossRef] [PubMed]

16. Lozinsky, V.I. Cryogels on the basis of natural and synthetic polymers: Preparation, properties and application. *Russ. Chem. Rev.* **2002**, *71*, 489–511. [CrossRef]

17. Lozinsky, V.I.; Galaev, I.Y.; Plieva, F.M.; Savina, I.N.; Jungvid, H.; Mattiasson, B. Polymeric cryogels as promising materials of biotechnological interest. *TRENDS Biotechnol.* **2003**, *21*, 445–451. [CrossRef]

18. Tripathi, A.; Kumar, A. Multi-featured macroporous agarose–alginate cryogel: Synthesis and characterization for bioengineering applications. *Macromol. Biosci.* **2011**, *11*, 22–35. [CrossRef]

19. Rodríguez-Dorado, R.; López-Iglesias, C.; García-González, C.A.; Auriemma, G.; Aquino, R.P.; Del Gaudio, P. Design of aerogels, cryogels and xerogels of alginate: Effect of molecular weight, gelation conditions and drying method on particles' micromeritics. *Molecules* **2019**, *24*, 1049. [CrossRef]

20. Bauleth-Ramos, T.; Shih, T.Y.; Shahbazi, M.A.; Najibi, A.J.; Mao, A.S.; Liu, D.; Granja, P.; Santos, H.A.; Sarmento, B.; Mooney, D.J. Acetalated dextran nanoparticles loaded into an injectable alginate cryogel for combined chemotherapy and cancer vaccination. *Adv. Funct. Mater.* **2019**, *29*, 1903686. [CrossRef]

21. Ciolacu, D.; Rudaz, C.; Vasilescu, M.; Budtova, T. Physically and chemically cross-linked cellulose cryogels: Structure, properties and application for controlled release. *Carbohydr. Polym.* **2016**, *151*, 392–400. [CrossRef]

22. Buchtová, N.; Pradille, C.; Bouvard, J.L.; Budtova, T. Mechanical properties of cellulose aerogels and cryogels. *Soft Matter.* **2019**, *15*, 7901–7908. [CrossRef] [PubMed]

23. Kathuria, N.; Tripathi, A.; Kar, K.K.; Kumar, A. Synthesis and characterization of elastic and macroporous chitosan–gelatin cryogels for tissue engineering. *Acta Biomater.* **2009**, *5*, 406–418. [CrossRef] [PubMed]

24. Bhat, S.; Tripathi, A.; Kumar, A. Supermacroporous chitosan–agarose–gelatin cryogels: In vitro characterization and in vivo assessment for cartilage tissue engineering. *J. R. Soc. Interface* **2011**, *8*, 540–554. [CrossRef] [PubMed]

25. Konovalova, M.V.; Markov, P.A.; Durnev, E.A.; Kurek, D.V.; Popov, S.V.; Varlamov, V.P. Preparation and biocompatibility evaluation of pectin and chitosan cryogels for biomedical application. *J. Biomed. Mater. Res. Part A* **2017**, *105*, 547–556. [CrossRef]

26. Han, M.E.; Kim, S.H.; Kim, H.D.; Yim, H.G.; Bencherif, S.A.; Kim, T.I.; Hwang, N.S. Extracellular matrix-based cryogels for cartilage tissue engineering. *Int. J. Biol. Macromol.* **2016**, *93*, 1410–1419. [CrossRef]

27. Yu, X.; Qian, G.; Chen, S.; Xu, D.; Zhao, X.; Du, C. A tracheal scaffold of gelatin-chondroitin sulfate-hyaluronan-polyvinyl alcohol with orientated porous structure. *Carbohydr. Polym.* **2017**, *159*, 20–28. [CrossRef]

28. Inci, I.; Kirsebom, H.; Galaev, I.Y.; Mattiasson, B.; Piskin, E. Gelatin cryogels crosslinked with oxidized dextran and containing freshly formed hydroxyapatite as potential bone tissue-engineering scaffolds. *J. Tissue Eng. Regen. Med.* **2013**, *7*, 584–588. [CrossRef] [PubMed]

29. Pacelli, S.; Di Muzio, L.; Paolicelli, P.; Fortunati, V.; Petralito, S.; Trilli, J.; Casadei, M.A. Dextran-polyethylene glycol cryogels as spongy scaffolds for drug delivery. *Int. J. Biol. Macromol.* **2021**, *166*, 1292–1300. [CrossRef]

30. Di Muzio, L.; Sergi, C.; Carriero, V.C.; Tirillò, J.; Adrover, A.; Messina, E.; Gaetani, R.; Petralito, S.; Casadei, M.A.; Paolicelli, P. Gelatin-based spongy and compressive resistant cryogels with shape recovery ability as ideal scaffolds to support cell adhesion for tissue regeneration. *React. Funct. Polym.* **2023**, *189*, 105607. [CrossRef]

31. Koshy, S.T.; Ferrante, T.C.; Lewin, S.A.; Mooney, D.J. Injectable, porous, and cell-responsive gelatin cryogels. *Biomaterials* **2014**, *35*, 2477–2487. [CrossRef]

32. Huang, Y.; Bai, L.; Yang, Y.; Yin, Z.; Guo, B. Biodegradable gelatin/silver nanoparticle composite cryogel with excellent antibacterial and antibiofilm activity and hemostasis for Pseudomonas aeruginosa-infected burn wound healing. *J. Colloid Interface Sci.* **2022**, *608*, 2278–2289. [CrossRef] [PubMed]

33. Baimenov, A.; Berillo, D.A.; Poulopoulos, S.G.; Inglezakis, V.J. A review of cryogels synthesis, characterization and applications on the removal of heavy metals from aqueous solutions. *Adv. Colloid Interface Sci.* **2020**, *276*, 102088. [CrossRef] [PubMed]

34. Berillo, D.; Al-Jwaid, A.; Caplin, J. Polymeric Materials Used for Immobilisation of Bacteria for the Bioremediation of Contaminants in Water. *Polymers* **2021**, *13*, 1073. [CrossRef] [PubMed]

35. Bhat, S.; Kumar, A. Cell proliferation on three-dimensional chitosan–agarose–gelatin cryogel scaffolds for tissue engineering applications. *J. Biosci. Bioeng.* **2012**, *114*, 663–670. [CrossRef] [PubMed]

36. Wartenberg, A.; Weisser, J.; Schnabelrauch, M. Glycosaminoglycan-Based Cryogels as Scaffolds for Cell Cultivation and Tissue Regeneration. *Molecules* **2021**, *26*, 5597. [CrossRef]

37. Yılmaz, F.; Bereli, N.; Yavuz, H.; Denizli, A. Supermacroporous hydrophobic affinity cryogels for protein chromatography. *Biochem. Eng. J.* **2009**, *43*, 272–279. [CrossRef]

38. Srivastava, A.; Shakya, A.K.; Kumar, A. Boronate affinity chromatography of cells and biomacromolecules using cryogel matrices. *Enzym. Microb. Technol.* **2012**, *51*, 373–381. [CrossRef]

39. Bereli, N.; Yavuz, H.; Denizli, A. Protein chromatography by molecular imprinted cryogels. *J. Liq. Chromatogr. Relat. Technol.* **2020**, *43*, 657–670. [CrossRef]

40. Memic, A.; Colombani, T.; Eggermont, L.J.; Rezaeeyazdi, M.; Steingold, J.; Rogers, Z.J.; Navare, K.J.; Mohammed, H.S.; Bencherif, S.A. Latest Advances in Cryogel Technology for Biomedical Applications. *Adv. Ther.* **2019**, *2*, 1800114. [CrossRef]

41. Siepmann, J.; Siepmann, F. Mathematical modeling of drug delivery. *Int. J. Pharm.* **2008**, *364*, 328–343. [CrossRef]

42. Lee, P.I. Kinetics of drug release from hydrogel matrices. *J. Control. Release* **1985**, *2*, 277–288. [CrossRef]

43. Singh, M.; Lumpkin, J.A.; Rosenblatt, J. Mathematical modeling of drug release from hydrogel matrices via a diffusion coupled with desorption mechanism. *J. Control. Release* **1994**, *32*, 17–25. [CrossRef]

44. Caccavo, D.; Cascone, S.; Lamberti, G.; Barba, A.A. Controlled drug release from hydrogel-based matrices: Experiments and modeling. *Int. J. Pharm.* **2015**, *486*, 144–152. [CrossRef] [PubMed]

45. Pacelli, S.; Paolicelli, P.; Avitabile, M.; Varani, G.; Di Muzio, L.; Cesa, S.; Tirillò, J.; Bartuli, C.; Nardoni, M.; Petralito, S.; et al. Design of a tunable nanocomposite double network hydrogel based on gellan gum for drug delivery applications. *Eur. Polym. J.* **2018**, *104*, 184–193. [CrossRef]

46. Caccavo, D.; Lamberti, G.; Barba, A.A. Mechanics and drug release from poroviscoelastic hydrogels: Experiments and modeling. *Eur. J. Pharm. Biopharm.* **2020**, *152*, 299–306. [CrossRef] [PubMed]

47. Dragan, E.S.; Dinu, M.V.; Ghiorghita, C.A.; Lazar, M.M.; Doroftei, F. Preparation and characterization of semi-IPN cryogels based on polyacrylamide and poly (N, N-dimethylaminoethyl methacrylate); Functionalization of carrier with monochlorotriazinyl-β-cyclodextrin and release kinetics of curcumin. *Molecules* **2021**, *26*, 6975. [CrossRef]

48. Groult, S.; Buwalda, S.; Budtova, T. Pectin hydrogels, aerogels, cryogels and xerogels: Influence of drying on structural and release properties. *Eur. Polym. J.* **2021**, *149*, 110386. [CrossRef]

49. Akbari, A.; Jafari, H.; Gohari, G.; Kheiri, G.; Mahdavinia, G.R. Fulvic acid-embedded poly (vinyl alcohol)–zinc oxide hydrogel nanocomposite: Synthesis, characterization, swelling and release kinetic. *Int. Nano Lett.* **2021**, *11*, 347–354. [CrossRef]

50. Szekalska, M.; Sosnowska, K.; Wróblewska, M.; Basa, A.; Winnicka, K. Does the freeze–thaw technique affect the properties of the alginate/chitosan glutamate gels with posaconazole as a model antifungal drug? *Int. J. Mol. Sci.* **2022**, *23*, 6775. [CrossRef]

51. Zagni, C.; Coco, A.; Mecca, T.; Curcuruto, G.; Patamia, V.; Mangano, K.; Rescifina, A.; Carroccio, S.C. Sponge-like macroporous cyclodextrin-based cryogels for controlled drug delivery. *Mater. Chem. Front.* **2023**, *7*, 2693–2705. [CrossRef]

52. Higuchi, T. Mechanism of sustained-action medication. Theoretical analysis of rate of release of solid drugs dispersed in solid matrices. *J. Pharm. Sci.* **1963**, *52*, 1145–1149. [CrossRef] [PubMed]

53. Korsmeyer, R.W.; Gurny, R.; Doelker, E.; Buri, P.; Peppas, N.A. Mechanisms of solute release from porous hydrophilic polymers. *Int. J. Pharm.* **1983**, *15*, 25–35. [CrossRef]

54. Ritger, P.L.; Peppas, N.A. A simple equation for description of solute release I. Fickian and non-fickian release from non-swellable devices in the form of slabs, spheres, cylinders or discs. *J. Control. Release* **1987**, *5*, 23–36. [CrossRef]

55. Ritger, P.L.; Peppas, N.A. A simple equation for description of solute release II. Fickian and anomalous release from swellable devices. *J. Control. Release* **1987**, *5*, 37–42. [CrossRef]

56. Georgiev, G.L.; Trzebicka, B.; Kostova, B.; Petrov, P.D. Super-macroporous dextran cryogels via UV-induced crosslinking: synthesis and characterization. *Polym. Int.* **2017**, *66*, 1306–1311. [CrossRef]

57. Ni, H.; Qian, S.; Lu, J.; Feng, J.; Mou, X.z.; Zhang, J. Natural Polysaccharide Delivery Platforms with Multiscale Structure Used for Cancer Chemoimmunotherapy. *Mol. Pharm.* **2023**, *20*, 5778–5789. [CrossRef] [PubMed]

58. Shiekh, P.A.; Andrabi, S.M.; Singh, A.; Majumder, S.; Kumar, A. Designing cryogels through cryostructuring of polymeric matrices for biomedical applications. *Eur. Polym. J.* **2021**, *144*, 110234. [CrossRef]

59. Bölgen, N.; Aguilar, M.R.; Fernández, M.D.M.; Gonzalo-Flores, S.; Villar-Rodil, S.; San, Román, J.; ; Pişkin, E. Thermoresponsive biodegradable HEMA–Lactate–Dextran-co-NIPA cryogels for controlled release of simvastatin. *Artif. Cells Nanomed. Biotechnol.* **2015**, *43*, 40–49. [CrossRef]

60. Slavkova, M.I.; Momekova, D.; Kostova, B.; Momekov, G.T.; Petrov, P. Novel dextran/β-cyclodextrin and dextran macroporous cryogels for topical delivery of curcumin in the treatment of cutaneous T-cell lymphoma. *Bulg. Chem. Commun* **2017**, *49*, 792–799.

61. Lei, D.; Zhao, J.; Zhu, C.; Jiang, M.; Ma, P.; Mi, Y.; Fan, D. Multifunctional Oxidized Dextran Cross-Linked Alkylated Chitosan/Drug-Loaded and Silver-Doped Mesoporous Bioactive Glass Cryogel for Hemostasis of Noncompressible Wounds. *Gels* **2023**, *9*, 455. [CrossRef]

62. Simon, L. A computational procedure for assessing the dynamic performance of diffusion-controlled transdermal delivery devices. *Pharmaceutics* **2011**, *3*, 485–496. [CrossRef] [PubMed]

63. Hauck, M.; Dittmann, J.; Zeller-Plumhoff, B.; Madurawala, R.; Hellmold, D.; Kubelt, C.; Synowitz, M.; Held-Feindt, J.; Adelung, R.; Wulfinghoff, S.; et al. Fabrication and Modelling of a Reservoir-Based Drug Delivery System for Customizable Release. *Pharmaceutics* **2022**, *14*, 777. [CrossRef] [PubMed]

64. Kalosakas, G.; Panagopoulou, E. Lag Time in Diffusion-Controlled Release Formulations Containing a Drug-Free Outer Layer. *Processes* **2022**, *10*, 2592. [CrossRef]

65. Van Dijk-Wolthuis, W.; Franssen, O.; Talsma, H.; Van Steenbergen, M.; Kettenes-Van Den Bosch, J.; Hennink, W. Synthesis, characterization, and polymerization of glycidyl methacrylate derivatized dextran. *Macromolecules* **1995**, *28*, 6317–6322. [CrossRef]

66. Di Muzio, L.; Paolicelli, P.; Brandelli, C.; Cesa, S.; Trilli, J.; Petralito, S.; Casadei, M.A. Injectable and in situ gelling dextran derivatives containing hydrolyzable groups for the delivery of large molecules. *Gels* **2021**, *7*, 150. [CrossRef] [PubMed]

67. Van Dijk-Wolthuls, W.; Tsang, S.; Kettenes-van den Bosch, W.E.; Hennink, J. A new class of polymerizable dextrans with hydrolyzable groups: Hydroxyethyl methacrylated dextran with and without oligolactate spacer. *Polymer* **1997**, *38*, 6235–6242. [CrossRef]

68. Maiti, S.; Maji, B.; Yadav, H. Progress on green crosslinking of polysaccharide hydrogels for drug delivery and tissue engineering applications. *Carbohydr. Polym.* **2023**, *326*, 121584. [CrossRef]

69. Alavarse, A.C.; Frachini, E.C.G.; da Silva, R.L.C.G.; Lima, V.H.; Shavandi, A.; Petri, D.F.S. Crosslinkers for polysaccharides and proteins: Synthesis conditions, mechanisms, and crosslinking efficiency, a review. *Int. J. Biol. Macromol.* **2022**, *202*, 558–596. [CrossRef]

70. Pumford, E.A.; Jackson Hoffman, B.A.; Kasko, A.M. Nontoxic Initiator Alternatives to TEMED for Redox Hydrogel Polymerization. *ACS Appl. Bio Mater.* **2024**, *7*, 2264–2271. [CrossRef]

71. Heller, M.C.; Carpenter, J.F.; Randolph, T.W. Application of a Thermodynamic Model to the Prediction of Phase Separations in Freeze-Concentrated Formulations for Protein Lyophilization. *Arch. Biochem. Biophys.* **1999**, *363*, 191–201. [CrossRef]

72. Adrover, A.; Varani, G.; Paolicelli, P.; Petralito, S.; Di Muzio, L.; Casadei, M.A.; Tho, I. Experimental and Modeling Study of Drug Release from HPMC-Based Erodible Oral Thin Films. *Pharmaceutics* **2018**, *10*, 222. [CrossRef]

73. Adrover, A.; Paolicelli, P.; Petralito, S.; Di Muzio, L.; Trilli, J.; Cesa, S.; Tho, I.; Casadei, M.A. Gellan Gum/Laponite Beads for the Modified Release of Drugs: Experimental and Modeling Study of Gastrointestinal Release. *Pharmaceutics* **2019**, *11*, 187. [CrossRef] [PubMed]